BULLETIN OF THE POLISH ACADEMY OF SCIENCES
TECHNICAL SCIENCES, Vol. 60, No. 3, 2012
DOI: 10.2478/v10175-012-0064-z

Active Disturbance Rejection Control of a 2DOF manipulator with significant modeling uncertainty

M. PRZYBYŁA, M. KORDASZ, R. MADOŃSKI, P. HERMAN, and P. SAUER*

Chair of Control and Systems Engineering, Faculty of Computing Science, Poznań University of Technology,
3a Piotrowo St., 61-138 Poznań, Poland

Abstract. This paper presents a practical verification of an Active Disturbance Rejection Control (ADRC) method in governing a multidimensional system. The experiments were conducted on a two degrees of a freedom planar manipulator with only partial knowledge about the mathematical model of the plant. This multi input multi output system was controlled with a set of two, independent, single input single output ADRC controllers, each regulating one of the manipulator degree of freedom. Modeling uncertainty (nonlinearities, cross-coupling effects, etc.) and external disturbances were assumed to be a part of the disturbance, to be estimated with an observer and cancelled on-line in the control loop. The ADRC robustness was experimentally compared with the results obtained from using two decentralized, classic PID controllers. Both control methods were tested under various conditions, e.g. changing the inertial parameters of the plant. Significantly better results, in terms of parametric robustness, have been reported for the ADRC approach.

Key words: ADRC, 2 DOF manipulator, modeling uncertainty.

1. Introduction

1.1. State of the art. One of the most fundamental research area in control theory and application is the study of disturbance rejection problem. Since most of the real environment systems unavoidably encounter disturbances, the goal is to use a control approach that will stay robust against the acting perturbation, while continue to effectively execute the desired task. Many methods, including adaptive and robust techniques, were proposed over the years to deal with this issue of both internal (i.e. related to the modeling uncertainty) and external disturbances in the system [1]. Despite the enormous work done in this subject, the mentioned control frameworks do not solve the problem entirely. The main reason is that most of them greatly depend on the mathematical model of the considered plant. In consequence, the quality of such model-based control systems rely directly on the accuracy of the assumed analytical description which, by the presence of for example nonlinearities and time-variant effects, is hard to obtain in engineering practice.

Some other techniques can be found in the literature that address the disturbance rejection problem by first trying to estimate the perturbation and then compensate its effects (a survey can be found in [2]). These techniques include Disturbance Observer [3], Unknown Input Observer [4], and Perturbation Observer [5]. The above methods are relatively simple to implement but are mostly dedicated to linear, time-invariant cases with an additional assumption that the precise mathematical description of the plant is somehow available. On the other hand, methods dedicated to nonlinear and time-variant plants include Model Estimator [2] technique and Time Delay Control [6]. They do not need a full analytical description of the plant but their main drawback is that they require information about higher order derivatives of the plant output signals, which can be problematic in some industrial situations.

Different approach for dealing with the system uncertainty, that does not poses the drawbacks mentioned above, is represented by an Active Disturbance Rejection Control method (or ADRC), proposed in [7, 8]. The ADRC is based on an extension of the system model with an additional and fictitious state variables, representing those elements of the system dynamics that the user does not include in the mathematical description of the plant. These virtual states (sum of internal and external disturbances, sometimes denoted as a *total disturbance*) are estimated on-line and used in the control loop in order to decouple the system from the actual perturbation acting on the plant. If the estimation procedure is accurate then this disturbance rejection feature allows user to treat the considered system with a simpler model, since the negative effects of modeling uncertainty are compensated in real time. As a result, the operator does not need a precise analytical description of the system, as one can assume the unknown parts of dynamics as the *total disturbance* influencing the plant. Robustness and the adaptive ability of this method makes it an interesting solution in scenarios where the knowledge of the system is not fully available.

The ADRC is a patented control framework that grows intensively in popularity. It was already proven to be a promising solution in various benchmark tests [9–11], as well as in practice [12–14]. The ADRC concept is also succesfully expanding in the industry, generally by a Cleveland State University spin-out company called LineStream Technologies[1]. Howev-

*e-mail: piotr.sauer@put.poznan.pl

[1]www.linestream.com

Unauthenticated | 89.67.242.59
Download Date | 5/19/13 8:28 PM

er, still a lot of research needs to be done regarding ADRC from both theoretical and practical points of view, since there are still some major disadvantages and unanswered questions regarding this approach.

1.2. Problem definition. One of the issue that still has to be addressed is the actual quality of ADRC approach in controling a complex MIMO systems without a precise modeling information. According to the authors best knowledge, there is no version of the ADRC dedicated strictly to multidimensional plants. Thus, it is interesting to investigate the applicability of decentralized version of ADRC to MIMO plants, where a set of controllers regulate each system degree of freedom seperetly.

Hence, in this work, we focus on the implementation of the decentalized version of ADRC algorithm for a two degrees of freedom (2DOF) laboratory manipulator[2] [15], with its mathematical model limited only to the knowledge of the system relative order. The cross-coupling effects in the considered 2DOF manipulator lead to an increase of the kinetic energy during the task realization, and for this reason, the use of proper control rule is crucial from practical point of view. The potential influence of the coupling phenomenon is treated in such framwework as a part of the acting external disturbance. In this study, the ADRC is compared with a classic model-free PID controller since the level of assumed system uncertainty in the considered 2DOF system effectively limits the possibility of using model-based control techniques (like Model Predictive Control or Feedback Linearizaion).

2. ADRC method

2.1. Basic idea. Instead of following a traditional modeling approach to obtain a mathematical expression of the acting disturbances, the ADRC method is an alternative that significantly reduces the dependence on explicit modeling. In ADRC, the necessary system information is obtained only through the input-output data of the considered plant. The information is acquired in each sampling time and is used by the feedback control system. Consequently, this control concept has the ability to react instantly against the *total disturbance* of the plant. In the ADRC framework, such disturbances are actively estimated using an Extended State Observer (or ESO) and further cancelled out in the control signal. Additionally, by rejecting the uncertainties in the system, task can be conducted effectively in the absence of the accurate mathematical model of the process.

Two main loops can be distinguished in the original ADRC concept: inner control loop (where the estimated disturbance is incorporated in the control signal) and outer control loop (where the reconstructed states are used in the output feedback controller).

2.2. State observer. The idea of ESO for estimating *total disturbance* can be demonstrated for a following single input single output n-th order plant:

$$y^{(n)} = \left[d_{int}\left(t, u, y, \dot{y}, \ddot{y}, \ldots, y^{(n-1)}\right) + d_{ext}\right] + bu = f + bu, \tag{1}$$

where y is the plant output signal, u is the plant input signal, d_{int} represents the overall internal disturbances (unmodeled system dynamics, parameter uncertainty, etc.), d_{ext} represents the overall external disturbances that affect the system, b denotes the system parameter, and f is the *total disturbance*[3]. The above plant can be rewritten using the assumed phase state variables (i.e. $x_1 = y$, $x_2 = \dot{y}$, ...) as:

$$\begin{cases} \dot{x}_1 = x_2 \\ \dot{x}_2 = x_3, \\ \vdots \\ \dot{x}_n = f + bu. \end{cases} \tag{2}$$

Assuming that f is m-times differentiable, the system from equation (2) can be augmented with other (also fictitious) state variables as seen below:

$$\begin{cases} \dot{x}_1 = x_2, \\ \dot{x}_2 = x_3, \\ \vdots \\ \dot{x}_n = x_{n+1} + bu, \\ \dot{x}_{n+1} = \dot{f}, \\ \dot{x}_{n+2} = \ddot{f}, \\ \vdots \\ \dot{x}_{n+m} = f^{(m)}, \end{cases} \tag{3}$$

where x_{n+1} is the *total disturbance* from equation (2) and $\dot{x}_{n+1}, \dot{x}_{n+2}, \ldots, \dot{x}_{n+m}$ are representing its consecutive time derivatives. Hence, choosing higher order of m allows user to reconstruct more complex disturbances, since the observer can track $(m-1)$-th order polynomial functions. On the other hand, high order ESO makes it more sensitive to noise and more difficult to tune.

The ESO, which in its linear version takes the form of a well-knwon Luenberger observer, can be designed to estimate states $x_1, x_2, \ldots, x_n, x_{n+1}, x_{n+2}, \ldots, x_{n+m}$:

$$\begin{cases} \dot{\widehat{x}}_1 = \widehat{x}_2 - \beta_1\,\epsilon, \\ \dot{\widehat{x}}_2 = \widehat{x}_3 - \beta_2\,\epsilon, \\ \vdots \\ \dot{\widehat{x}}_n = \widehat{x}_{n+1} - \beta_n\,\epsilon + \widehat{b}u, \\ \dot{\widehat{x}}_{n+1} = \widehat{x}_{n+2} - \beta_{n+1}\,\epsilon, \\ \dot{\widehat{x}}_{n+2} = \widehat{x}_{n+3} - \beta_{n+2}\,\epsilon, \\ \vdots \\ \dot{\widehat{x}}_{n+m} = -\beta_{n+m}\,\epsilon, \end{cases} \tag{4}$$

[2]The work is a continuation and development of the research started in [15], where parametric robustness tests were performed on a 1DOF manipulator.
[3]As mentioned before, we assume that we do not have any knowledge about the system, only its relative degree of freedom (n).

Unauthenticated | 89.67.242.59
Download Date | 5/19/13 8:28 PM

where $\beta_1, \beta_2, \ldots, \beta_n, \beta_{n+1}, \beta_{n+2}, \ldots, \beta_{n+m}$ are the observer gains, $\epsilon := y - \widehat{x}_1$ stands for the estimation error of state x_1, and $\widehat{b}$ is an estimation of parameter b from equation (1), usually chosen explicitly by the user.

2.3. Feedback controller. The control goal is to obtain proper estimation and then cancellation of the *total disturbance* along with the assurence of satysfying trajectory tracking. The governing signal in the traditional ADRC is defined as follows:

$$u := \frac{-\widehat{x}_{n+1} + \overline{u}}{\widehat{b}}, \tag{5}$$

where $\overline{u}$ is the output signal from a feedback controller. The type of controller in ADRC is optional, but should be related to a given task and the desired closed-loop behavior of the system. One can notice that the $\widehat{b}$ parameter scales the dynamics of the controller since it shapes the denominator of the above control rule. Assuming the proper estimation of b (i.e. $\widehat{b} \approx b$) and *total disturbance* (i.e. $\widehat{x}_{n+1} \approx f$) we can idealistically assume that:

$$y^{(n)} = f + bu = f + b\left(\frac{-\widehat{x}_{n+1} + \overline{u}}{\widehat{b}}\right) \approx \overline{u}. \tag{6}$$

The complex system from equation (2) can now be expressed with a simpler and disturbance-free theoretical equation (6), which in the considered example reduced the initial system (1) to just a set of linear integrators, which can be effectively governed with some classical linear control designs [1]:

$$\begin{cases} \dot{x}_1 = x_2, \\ \dot{x}_2 = x_3, \\ \vdots \\ \dot{x}_n = \overline{u}. \end{cases} \tag{7}$$

2.4. ESO parameterization. The ESO gains can be found using a simple pole-placement method (as presented in [16]), where the roots of a characteristic polynomial:

$$\begin{aligned} \lambda(s) &= s^{n+m} + \beta_1\, s^{n+m-1} + \beta_2\, s^{n+m-2} \\ &+ \ldots + \beta_{n+m-2}\, s^2 + \beta_{n+m-1}\, s + \beta_{n+m} \end{aligned} \tag{8}$$

are compared to a following polynomial:

$$G(s) = (s + \omega_0)^{n+m}, \tag{9}$$

which places all of the observers poles in the left half plane at $-\omega_0$, making the characteristic polynomial a Hurwitz-type. The overall performance of ADRC is thus highy related to the state reconstruction phase, that is why the observer gains have to be chosen large (in practice however, a compromise has to be made between estimation quality and noise filtering). When implementing ADRC, the user has to remember to start the tuning procedure with the observer. Once the state estimation is satisfactory, the operator can begin to tune the feedback control loop. Thanks to the separation principle, observer and controller tuning can take place independently. The $(n+m)$-th order ESO with an exemplary feedback control scheme is presented on Fig. 1, where y_d is the reference signal.

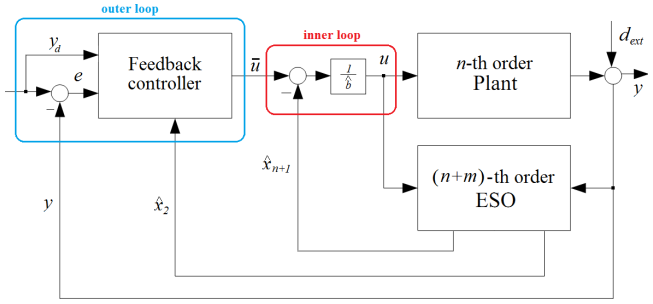

Fig. 1. Exemplary n-th order plant with the feedback controller and the $(n+m)$-th order ESO.

2.5. Comments on stability. Although the ADRC has demonstrated its advantages in many practical applications (mentioned in previous section), its full theoretical analysis is still an open problem. However, some interesting contribution can be pointed out at this time as well.

In [17], the stability of ESO and the whole ADRC was considered. It was proven there, that with a given plant dynamics, the system describing the estimation error in ESO is asymptotically stable. It was also shown that with a plant mathematical description largely unknown, the ESO can estimate the unmodeled dynamics and disturbances. Additionally, the estimation error upper bound of the ESO monotonously decreases with the observer bandwidth. Moreover, the closed-loop system based on ADRC was shown to be asymptotically stable when the plant model was given. But with the plant dynamics largely unknown, the tracking error in ADRC and its up to $(n-1)$-th order derivatives were shown to be bounded and their upper bounds monotonously decrease with the observer and controller bandwidths.

In [18], by the use of a singular perturbation method, the observer error and the tracking error of the system were proven to be exponentially stable. Bounded input and bounded output stability was suggested in [19] and the frequency domain stability analysis for linear plants was presented in [20]. The convergence and the bounds of the both estimation error and tracking error were also presented in [21]. In [22], boundedness of all variables of the closed-loop system in the presence of modeling uncertainty and time-varying disturbance was guaranteed with a nonlinear version of ESO.

3. System description

To bring closer the rationale of proceeded experiment, the working principles as well as the analytical model of the considered plant are introduced below. The planar manipulator with two rotational joints (PM2R, details in [23]) used in the tests was designed by a research group affiliated with the Chair of Control and Systems Engineering[4] from the Poznań University of Technology.

[4]www.control.put.poznan.pl

Unauthenticated | 89.67.242.59
Download Date | 5/19/13 8:28 PM

3.1. Physical characteristics. The PM2R is seen in Fig. 2. Its axes of rotation run parallel to each other and perpendicular to the gravity vector. Lengths of the links are equal to $L_1 = 0.25$ m and $L_2 = 0.18$ m. The area of reachability of the end effector is thus a ring of outer radius $R_{out} = L_1 + L_2 = 0.43$ m and inner radius $R_{inn} = L_1 - L_2 = 0.07$ m.

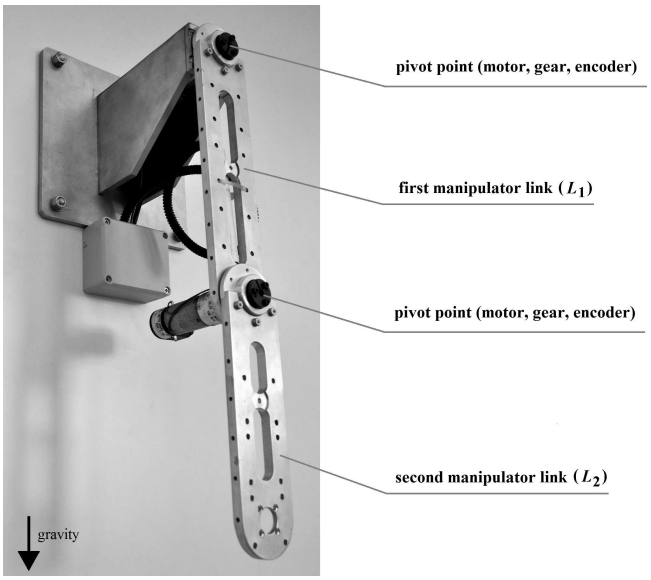

Fig. 2. The PM2R manipulator with the assumed notation.

Each of the joint is driven with a 12 V DC motor with a planetary gear attached to the shaft. The reduction ratios of the gears are equal to $\eta_1 = 1/36$ and $\eta_2 = 1/20.25$ respectively. In order to preserve the motors from damage due to supertension, an artificial voltage saturation of value $|U_{sat}| = 12$ V is set in the controller. It results in system nonholonomic constraints (i.e. the velocities are bounded) which introduce additional signal uncertainty. On each motor shaft, an impulse encoder of resolution $p = 500\ \frac{\text{imp}}{\text{rev}}$ is mounted. The control system is implemented on a TMS320F2812 fixed-point DSP board with constant sampling rate set to $T_s = 0.0011$ s. The initial point of the end effector (equal to the natural stable point, congruent with the minimal potential energy of the system) is situated in $X_{\min}$ [m] $= (0, -L_1 - L_2)$. This point is achieved with the $q_{\min}$ [rad] $= (0,\ 0)$ configuration.

3.2. Mathematical model. The input signals of PM2R are the voltages u_{m1} [V] and u_{m2} [V] provided for each of the two DC motors driving the links. The output signals of the system are the angular positions q_{m1} [rad] and q_{m2} [rad] of the motor shafts. In general, the model of PM2R can be written as two scalar equations concerning each of the manipulator's links:

$$I_j \ddot{q}_{mj} + f_j = \tau_{mj} + \tau_{zj} - \tau_{cj}, \quad \text{for j} = \{1, 2\}, \tag{10}$$

where I_j [kg m^2] denotes the inertia part of the model, f_j [Nm] presents the friction model, τ_{mj} [Nm], τ_{zj} [Nm], and τ_{cj} [Nm] are the driving torques, disturbance torques and cross-coupling torques respectively.

By introducing the dynamical parameters p_1 – p_5 as in Table 1:

Table 1
Dynamical parameters of the PM2R model

p_1 [kg m^2]	$m_2 L_2^2 + J_2$
p_2 [kg m^2]	$2m_2 L_1 L_2$
p_3 [kg m^2]	$J_1 + m_1 L_1^2 + 4m_2 L_1^2$
p_4 [Nm]	$m_2 L_2 g$
p_5 [Nm]	$(m_1 L_1 + 2m_2 L_1) g$

where m_j [kg], J_j [kg m^2] are the mass and moment of inertia of j-th link respectively, $g\ \left[\frac{\text{m}}{\text{s}^2}\right]$ is the gravitational acceleration, the inertia part for the PM2R links can be described as:

$$\begin{aligned} I_1 &= J_{m1} + \eta_1^2 (p_1 + p_3), \\ I_2 &= J_{m2} + \eta_2^2 (p_2). \end{aligned} \tag{11}$$

Here, J_{mj} [kg m^2] is the moment of inertia of the j-th motor shaft. The friction model consist of joint as well as motor shaft friction. The cross-couplings influence is given by:

$$\begin{aligned} \tau_{c1} &= \eta_1 \ddot{q}_{m1} p_2 c_{m1} + \eta_2 \ddot{q}_{m2} p_2 c_{m2} - \eta_1 \dot{q}_{m1} \eta_2 \dot{q}_{m2} p_2 s_{m2} \\ &\quad - \eta_2 \dot{q}_{m2} p_2 (\eta_1 \dot{q}_{m1} + \eta_2 \dot{q}_{m2}) s_{m2} + p_5 c_1 + p_4 c_{m12}\ , \\ \tau_{c2} &= (p_1 + p_2 c_2) \eta_2 \ddot{q}_{m2} + \eta_2^2 \dot{q}_{m1}^2 p_2 s_{m2} + p_4 c_{m12}\ , \end{aligned} \tag{12}$$

where, for simplicity $s_{m1} \equiv \sin(q_{m1})$, $c_{m1} \equiv \cos(q_{m1})$ and $c_{m12} \equiv \cos(q_{m1} + q_{m2})$.

The driving torques stem directly from the electromechanical model of the DC motors and can be simplified to:

$$\tau_{mj} = \frac{k_{Ij}}{R_j} (u_{mj} - k_{\epsilon j} \dot{q}_{mj}), \tag{13}$$

where k_{Ij} $\left[\frac{\text{Nm}}{\text{A}}\right]$ is the j-th motor's torque constant, $k_{\epsilon j}$ $\left[\frac{\text{V s}}{\text{rad}}\right]$ is the j-th motor's speed constant and R_j [Ω] is the j-th motor's coil electrical resistance. Note that the motor inductance was ignored because of its to low importance.

By presenting the analytical model of the system, we try to emphasize the difficulties concerning working with model-based control methods (e.g. the amount of parameters to be known or identified). A precise model itself will not be used in the presented control algorithms.

4. Application of ADRC method to PM2R manipulator

For the sake of design simplicity and further tuning, following assumptions were made:

A1 According to our best knowledge, there is no multi input multi output version of ADRC available at this time. Hence, one independent controller for each degree of freedom (i.e. each DC motor driving the link) was designed. Therefore, the considered control system is a set of second order SISO controllers each governing one dimension of the plant. In such approach, we treat the cross-couplings effects as part of the external disturbance.

Unauthenticated | 89.67.242.59
Download Date | 5/19/13 8:28 PM

A2 No information about the system parameters is given. Only the relative degree of each SISO part of the 2DOF plant is known (i.e. $n = 2$). Additionally, both input and output signals of the PM2R are available by direct measurement.

A3 The first derivative of *total disturbance* equals zero (i.e. $m = 1$, see Sec. 2). This may look like a strong assumption, that we consider the perturbation to be constant. However, it was shown in [24] that the ADRC has great capabilities of estimation different types of disturbances (e.g. constant, square, sinusoidal), even when $m = 1$.

A4 In order to implement the ADRC on DSP board, a backward Euler discretization method was used. However, for clarity of presentation, the upcoming mathematical deliberations will be given in continuous form.

By assuming following phase state variable $x_{11} = q_{m1}$, the mathematical model of the first link from equation (10), can be rewritten as:

$$\begin{cases} \dot{x}_{11} = x_{21}, \\ \dot{x}_{21} = f_1(\cdot) + b_1 u_{m1}, \end{cases} \tag{14}$$

where f_1 is the assumed *total disturbance* of the system, which is a sum of all the uncertainties of the considered system and b_1 is a system variable[5].

The extended model, consisting of an extra state (i.e. x_3) representing the *total disturbance*, is presented below:

$$\begin{cases} \dot{x}_{11} = x_{21}, \\ \dot{x}_{21} = x_{31} + b_1\, u_{m1}, \quad x_{31} = f_1, \\ \dot{x}_{31} = \dot{f}_1. \end{cases} \tag{15}$$

Now, a following third order ESO is designed for the above system:

$$\begin{cases} \dot{\widehat{x}}_{11} = \widehat{x}_{21} - \beta_{11}\, \epsilon_1, \\ \dot{\widehat{x}}_{21} = \widehat{x}_{31} - \beta_{21}\, \epsilon_1 + \widehat{b}_1\, u_{m1}, \\ \dot{\widehat{x}}_{31} = -\beta_{31}\, \epsilon_1. \end{cases} \tag{16}$$

The control signal of the first motor is described with a following equation:

$$u_{m1} = \frac{-\widehat{x}_{31} + \overline{u}_1}{\widehat{b}_1}. \tag{17}$$

A simple PD controller (denoted as $\overline{u}_1$) was chosen for each ADRC control loop. Assuming the proper estimations of b_1 (i.e. $\widehat{b}_1 \approx b_1$) and the *total disturbance* (i.e. $\widehat{x}_{31} \approx f_1$) one can assume that:

$$\ddot{q}_{m1} = f_1 + b_1\, u_{m1} = f_1 + b_1 \left(\frac{-\widehat{x}_{31} + \overline{u}_1}{\widehat{b}_1} \right) \approx \overline{u}_1. \tag{18}$$

The complex system described by equation (10) can now be expressed with a simpler and disturbance-free equation (18) which is a set of the following linear integrators:

$$\begin{cases} \dot{x}_{11} = x_{21}, \\ \dot{x}_{21} = \overline{u}_1, \\ y = x_1. \end{cases} \tag{19}$$

The above reduced model can be rewritten using tracking error:

$$\begin{cases} e_1 = x_{d11} - x_{11}, \\ \dot{e}_1 = \dot{x}_{d11} - \dot{x}_{11} = x_{d21} - x_{21}, \\ \ddot{e}_1 = \dot{x}_{d21} - \dot{x}_{21} = \ddot{x}_{d11} - \overline{u}_1, \end{cases} \tag{20}$$

where x_{d11} is the desired value of state x_{11}, element x_{d21} is the desired value of state x_{21}. In the above formula, element $\overline{u}_1$ is the feedback controller responsible for minimizing the tracking error:

$$\overline{u}_1 = \ddot{x}_{d11} + u_{sf1} = \ddot{x}_{d11} + [k_{p1}\ k_{d1}]\,[e_1\ \dot{e_1}]^T, \tag{21}$$

where $\ddot{x}_{d11}$ is the feed-forward signal[6], u_{sf1} is the feedback part (we considered it as a PD controller), k_{p1} is the proportional gain, k_{d1} is the derivative gain, error and its derivative are defined as $e = q_{md1} - q_{m1}$ and $\dot{e} = \dot{q}_{md1} - \widehat{x}_{21}$, respectively. Signal q_{m1} is available by the use of an encoder, placed on the motor shaft.

By applying equation (21) to the third term in (20) we obtain a following error dynamics equation:

$$\ddot{e}_1 + k_{d1}\dot{e}_1 + k_{p1}e_1 = 0. \tag{22}$$

By choosing proper k_{p1} and k_{d1} gains we can obtain the exponential convergence of the tracking error to zero for any initial conditions.

Consideration, similar to the one above, can be done for the second manipulator link. It will result in two separate ADRC controllers, one for each dimension of the system. The full ADRC control scheme for the PM2R system is presented on Fig. 3. The tuning of such control system will be presented later on. Similar observer parametrization to the one seen in Subsec. 2.3 was used for the purpose of the experiment.

[5]Usually, this parameter is considered to be constant, however when dealing with cross-coupled systems the parameter varies in time, since it is in this case a function of q_{m2}, $\dot{q}_{m2}$, and $\ddot{q}_{m2}$.

[6]We assumed in the implementation that this element is unavailable.

Unauthenticated | 89.67.242.59
Download Date | 5/19/13 8:28 PM

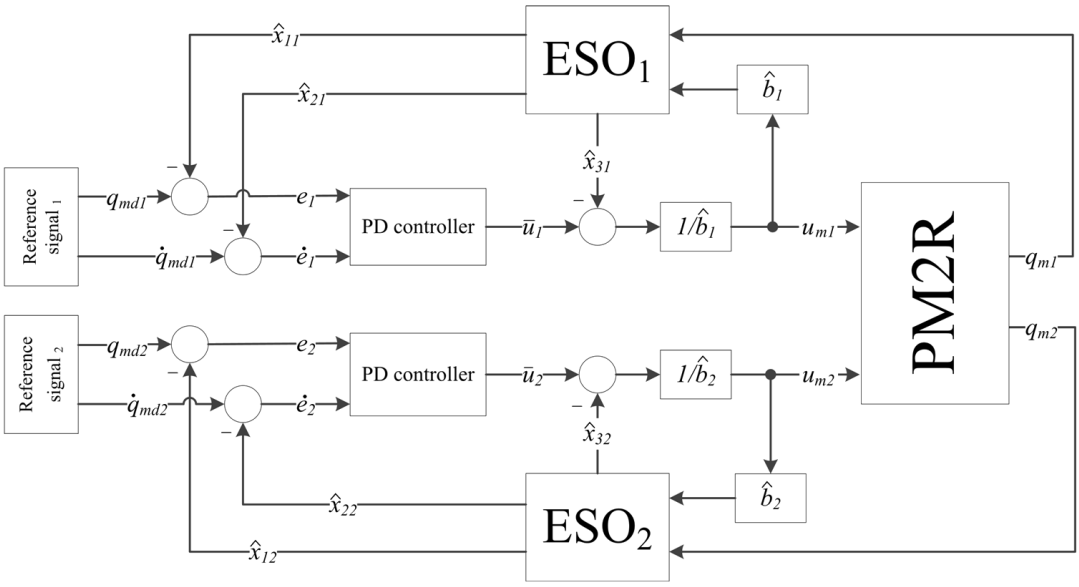

Fig. 3. Block diagram of the decentralized ADRC design for the PM2R system.

5. Trajectory planning

Planning a reference trajectory in the Cartesian space for a 2DOF manipulator is not a trivial task. At first, the geometry of the designed path must be chosen on the two dimensional plane X,Y$\in R^2$. Then, the path is parametrized with time, i.e. the velocities are considered, generating the designed trajectory. Finally, on the basis of previous calculation and an inverse kinematics method, the Cartesian space trajectory is projected into robot state space.

Two different trajectories must be distinguished: the designed trajectory (i.e. generated on the basis of the ideal shape path, developed by the designer) and the reference trajectory (i.e. the result of inverse kinematics process). Comparison between the designed trajectory and the reference trajectory is presented on Fig. 4.

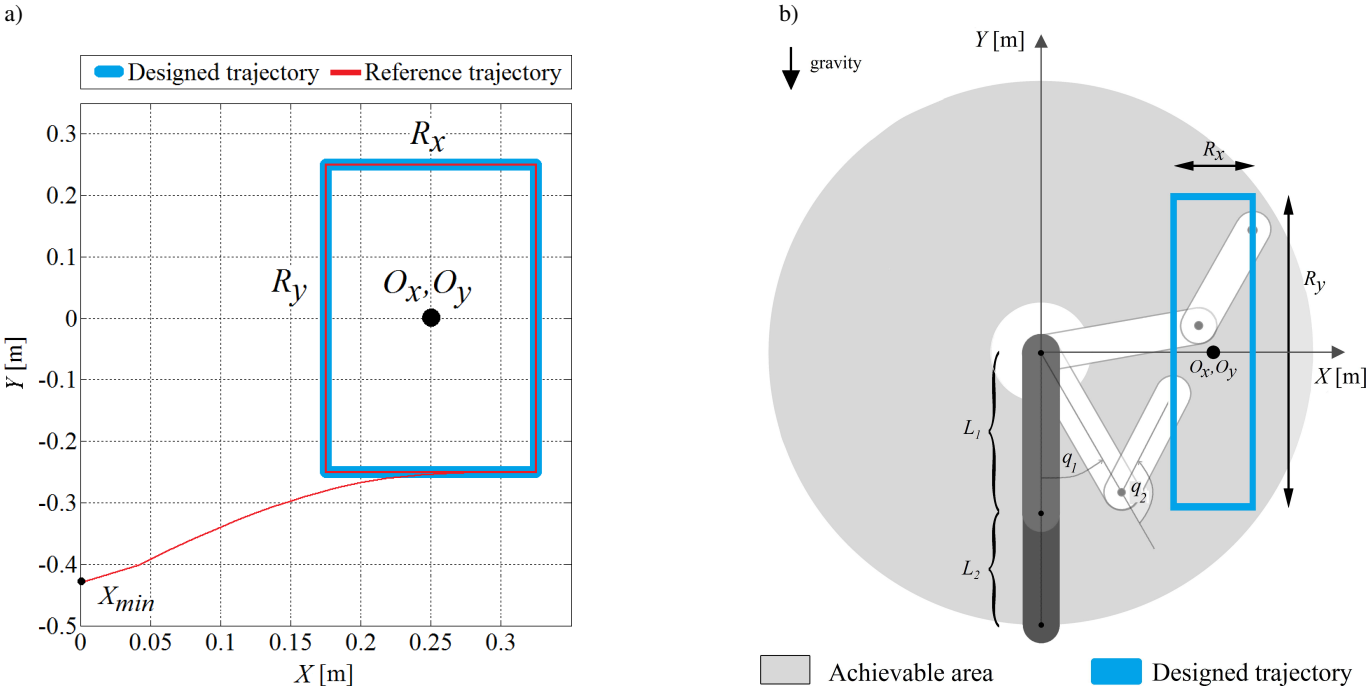

Fig. 4. Differences between "designed" and "reference" trajectories for the robot end effector (a) and a schematic interpretation of the manipulator with the designed trajectory (b).

Unauthenticated | 89.67.242.59
Download Date | 5/19/13 8:28 PM

Additionally, we use traditional notation, where the trajectory is a path with extra time regime.

5.1. Designed path and trajectory. Designed path is represented in the Cartesian space in which the end effector moves along the rectangle border (Fig. 4). The path's central point coordinates are $O_x = 0.25$ m, $O_y = 0$ m, and the lengths of horizontal and vertical sections are $R_x = 0.15$ m, $R_y = 0.5$ m respectively. The designed trajectory is given by the following parameters. Execution time of one cycle (i.e. each of four sections on Fig. 4) equals $T = 6$ s. Each of the four sections of the rectangular reference path is executed within the same amount of time, i.e. $T_{sec} = \frac{T}{4}$ s, thus the velocities along longer segments have greater values than the ones along shorter segments[7].

The trajectory of each segment is designed as a standard Linear Segments with Parabolic Blends (LSPB) trajectory. The blend time is equal to $T_b = \frac{T}{24}$ and the maximum velocity is calculated as:

$$V_{max} = \frac{d}{T - T_b}, \tag{23}$$

where d [m] describes the length of a section (i.e. R_x or R_y). The velocity of the end effector along the single section is given by the trapezoid shape.

It is also worth noticing, that the designed trajectory start point should be chosen as close as possible to the natural manipulator state. With control system, properly chosen and tuned, the error will converge quickly but within first seconds the transitional state can be crucial for the plant working conditions.

Note that following the path presented on Fig. 4 is a very demanding task, since it covers points situated close to manipulator achievable area border. Additionally, the influence of the gravity vector is increasing while moving along vertical segments of a given path, as it is either decelerating or accelerating the end effector.

5.2. Inverse kinematics To plan a trajectory in the Cartesian space, obtaining the desired state-space signals is necessary, hence the inverse kinematics needs to be implemented. In general, this task is not trivial because of ambiguous solutions obtained by calculations. That is, most of the end effector positions can be achieved with more than one state configuration.

As a solution, a Jacobian method is used to produce the state-space trajectory. This closed loop system involves the direct kinematics mechanism in the feedback loop and inverse Jacobie matrix in the main loop. Direct kinematics is described with the following equations:

$$\begin{aligned} x &= L_1 \sin(q_1) + L_2 \sin(q_1 + q_2), \\ y &= -L_1 \cos(q_1) - L_2 \cos(q_1 + q_2). \end{aligned} \tag{24}$$

The above equation calculates coordinates x [m] and y [m] of the end effector from state configuration q_1 [rad] and q_2 [rad]. The analytical Jacobian matrix for considered system is presented below:

$$\boldsymbol{J}_A = \begin{bmatrix} L_1 c_1 + L_2 c_{12} & L_2 c_{12} \\ L_1 s_1 + L_2 s_{12} & L_2 s_{12} \end{bmatrix}, \tag{25}$$

where s_1, c_1, s_{12} and c_{12} are abridged notations of $\sin(q_1)$, $\cos(q_1)$, $\sin(q_1 + q_2)$ and $\cos(q_1 + q_2)$ respectively. Multiplication of the matrix from (25) and angular velocities $\dot{\boldsymbol{q}} = [\dot{q}_1 \ \dot{q}_2]^T$ of the joints gives the velocity vector of the end effector $\boldsymbol{v} = [\dot{x} \ \dot{y}]^T$. Inversion of this matrix leads to equation:

$$\dot{\boldsymbol{q}} = \boldsymbol{J}_A^{-1} \boldsymbol{v}. \tag{26}$$

In some cases, the J_A matrix appears to be singular, so then the inversion procedure is impossible. The phenomenon appears only for short time periods. That is why, it is important to implement a security rule in which the angular velocities stay constant until Jacobie matrix leaves singularity region.

Finally, the Jacobian inverse kinematics method is described with:

$$\dot{\boldsymbol{q}} = \boldsymbol{J}_A^{-1} \left(\boldsymbol{v}_d + \alpha \left(\boldsymbol{x}_d - \boldsymbol{x} \right) \right), \tag{27}$$

where the α parameter is an additional error gain, and was set to 5 Hz. For the sake of clarity, the inverse kinematics system is additionally depicted on Fig. 5.

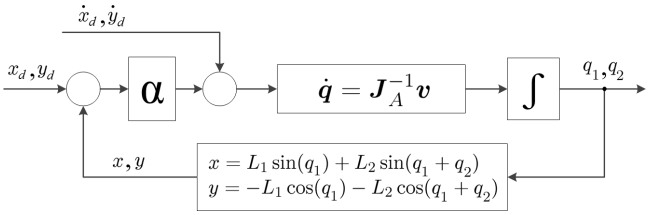

Fig. 5. The Jacobian method scheme.

6. Experiment preparation

The aim of the tests is the practical verification of the ADRC method in controling the multidimensional plant with the lack of precise modeling. Hence, the experiment is divided into two following cases:

E1 In the first part, we tune ADRC and PID for the "pure" PM2R mechanism (i.e. no additional mass attached on the end effector), described in Sec. 3. The goal here is to aquire similar control quality in terms of desired path tracking with the presence of highly unknown and unpredictible phenomena.

E2 In the second part, we mount an additional mass $m_{add} = 0.2$ kg to the end effector and without any additional retuning after case E1 we test both of the control systems again. The objective is to examine the parametric robustness of the ADRC and PID in the case of increasing the moment of link inertia.

[7] Various velocities provide a better outlook on control system's behavior in different situations. This action is deliberate.

Unauthenticated | 89.67.242.59
Download Date | 5/19/13 8:28 PM

6.1. Tuning process. Both of the considered controllers were tuned empirically with the goal to provide the best control quality (in terms of minimization of the tracking error without significant output signal overshoot). It is not trivial to find proper tuning parameters for MIMO system, especially with the influence of cross-coupling effct and the lack of plant full mathematical description. Hence, for both of the considered controllers an intuitive and model-free technique was used and is described next[8].

In the PID approach, three parameters (proportional, integral, and derivative gains) for each control dimension had to be chosen, namely: k_{p1}, k_{i1}, k_{d1}, and k_{p2}, k_{i2}, k_{d2}. The tuning procedure started with only the proportional term being increased until the desired level of output signal was obtained with not more than 10% output signal overshoot. Next, the derivative gain was implemented to compensate the overshoot. The integrating action was also added to limit the possible steady-state error effect, even though it was hard to observe because of the constant movement of the second joint and its reaction on the whole system.

For the ADRC, we introduced a parametrization technique to reduce the number of parameters in the tuning procedure (see Subsec. 2.3). Nevertheless, four parameters still had to be chosen for each ADRC controller, namely: k_{p1}, k_{d1}, ω_1, $\widehat{b}_1$, and k_{p2}, k_{d2}, ω_2, $\widehat{b}_2$. We should notice that even though in the ADRC, the observer and the controller can be tuned independently (by the virtue of separation principle), the user should start the tuning process with the observer since the observer works in inner loop of the whole feedback control systems. The ESO can be easily tuned in the considered setup by manualy moving each joint in the both motors idle modes. Once the ESO is estimating all the needed signals with satisfying quality and without unacceptable measurement noises in the higher state variables, then the tunning process of the PD feedback controller can begin. Here, the tuning approach is similar to the one in PID, however the integrating element is omitted since it is already included in the structure of the proposed state observer. Parameters chosen for the PID and ADRC method are in Tables 2 and 3:

Table 2
The PID tuning parameters

$k_{p1} = 150$	$k_{i1} = 1$	$k_{d2} = 2$
$k_{p2} = 150$	$k_{i2} = 1$	$k_{d2} = 2$

Table 3
The ADRC tuning parameters

$k_{p1} = 150$	$k_{d1} = 4$	$\omega_1 = 12.5$	$\widehat{b}_1 = 2$
$k_{p2} = 150$	$k_{d2} = 4$	$\omega_2 = 9$	$\widehat{b}_2 = 2$

6.2. Polar coordinates error. In order to depict results in more intuitive way, a polar coordinates error is introduced. The polar error directly shows the modulus (ρ [rad]) and phase (φ [m]) errors, which can be interpreted as errors in space and time. The joint space error as well as the error in the Cartesian space do not have to be as evident in its importance as the polar coordinates error.

We choose the pole to be the central point, i.e. (O_x, O_y). The error is described with following equations:

$$\begin{aligned} e_\rho &= \rho_d - \rho, \\ e_\varphi &= \varphi_d - \varphi, \end{aligned} \tag{28}$$

where ρ_d [m] and ρ [m] describe the desired and the actual trajectory modulus respectively, while φ_d [rad] and φ [rad] represent the desired and the actual trajectory phase, respectively. They are obtained with the equations seen below:

$$\begin{aligned} \rho &= \sqrt{(x - O_x)^2 + (y - O_y)^2}, \\ \varphi &= \mathrm{atan2c}\left(\mathrm{y} - \mathrm{O_y},\ \mathrm{x} - \mathrm{O_x}\right), \end{aligned} \tag{29}$$

where $\mathrm{atan2c}(\cdot) : \Re^2 \to \Re$ is a two argument, continuous version of arcus tangent function.

6.3. Curvature Projection Error. In the upcoming experiments, we also tested the controllers in a path tracking task. It is justified by the fact that the path is more intuitive to analyze than trajectory[9]. To depict the quality of path following in means of shape projection, a Curvature Projection Error (CPE) is introduced. The CPE is calculated for each point of the end effector achieved path. All points of the path are subscribed to one of four groups of points, each representing one side of the designed path rectangle. The CPE denotes the distance between the point of the achieved path and the closest point in designed path, with an assumption that both points ought to be located in the same group.

Assume that an exemplary point on the path performed by the end effector is given by the following Cartesian coordinates $P = (P_x, P_y)$. Point on the reference path, which is the nearest to the point P and is a part of equivalent group, is given by: $P_{ref} = (P_{x_{ref}}, P_{y_{ref}})$. The CPE graph shows the minimal distances between points P and P_{ref} for all samples of the actual path:

$$CPE = \sqrt{(P_x - P_{x_{ref}})^2 + (P_y - P_{y_{ref}})^2}. \tag{30}$$

On the basis of CPE graph, a simple root mean square (RMS) is calculated to measure the magnitude of a varying quantity of the CPE:

$$CPE_{RMS} = \sqrt{\frac{1}{N}\sum_{i=1}^{N} CPE^2}, \tag{31}$$

where N is the number of samples of the end effector path. Desirably, the CPE should be in close neighborhood of zero.

To emphasize the differences in realization of the path following task, the CPE as well as its root mean square, will be described in millimeters (contrary to the 2D position of the end effector, which is expressed in meters).

[8] Such empirical tuning approach was also successfully implemented in [9, 10, 15] and [23].
[9] In this case, we analyze the curvature following in spite of time imposition.

Unauthenticated | 89.67.242.59
Download Date | 5/19/13 8:28 PM

7. Experimental results

Conducted tests provided us with better understanding of the performance of both considered controllers in terms of path following, trajectory tracking, and energy efficiency (in means of control signal). In this section, we present the obtained results for two performed experiments, denoted as E1 and E2.

7.1. System with basic mass (E1). The graph comparing the designed trajectory with trajectories achieved for both control algorithms is presented on Fig. 6. No significant difficulties can be seen here, for PID as well as for ADRC. Both control strategies ensure reaching the designed trajectory from the initial point and efficiently following it. For more detailed analysis, we have examined three different aspects of controller performance separately, namely: path error, trajectory error, and control signal.

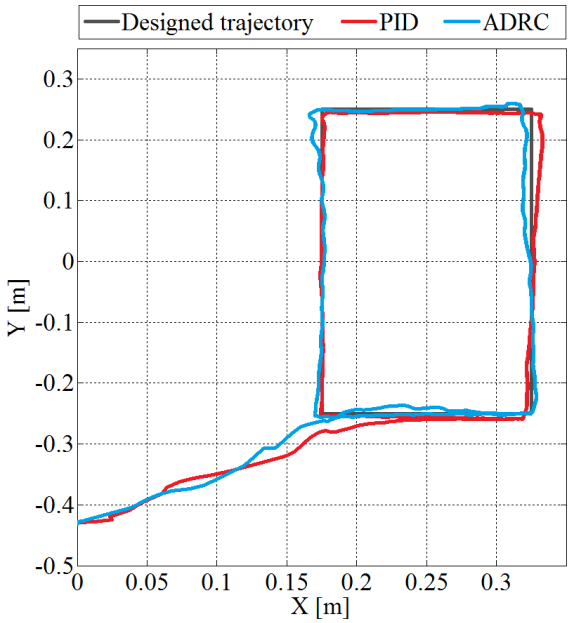

Fig. 6. Designed trajectory and actual trajectories obtained for both of the controllers in the case of system with basic mass (E1)

Path error. In order to visualize the quality of path tracking, the CPE is presented on Fig. 7. Only one segment of whole path is shown on the plot. As it can be deduced from the graph, both controllers guaranteed that CPE was within ± 10 mm tunnel for each sample of the experiment. Therefore, the shape of designed path is accurately copied. However, ADRC seems to be more efficient, what is proven by the CPE_{RMS} values. For the PID it is equal 4.86 mm and for ADRC it is 3.55 mm.

Trajectory error. Neglecting the transitional state, both: ADRC and PID do not exceed $\pm 1 \times 10^{-2}$ m deviation from the designed trajectory. The modulus error, shown on Fig. 8, confirm this characteristic. The error of ADRC is correlated to figure's geometry, i.e. it reaches its extreme values while passing the corners. The PID on the other hand, is repetitive over the whole cycle, not over a single section of motion. Also, the ADRC modulus error is bound within smaller area as compared to PID.

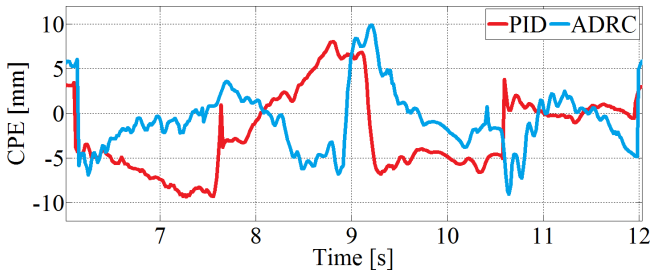

Fig. 7. Curvature projection error in the case of system with basic mass (E1)

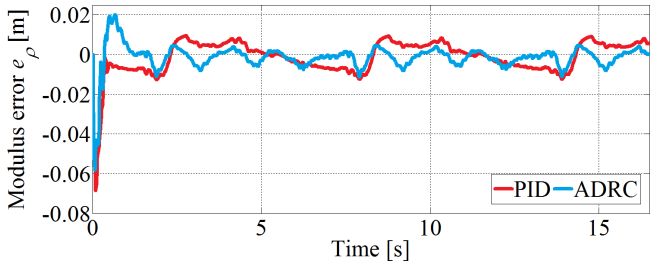

Fig. 8. Modulus error e_ρ for the system with basic mass (E1)

The phase errors are depicted on Fig. 9. The positive value of phase error means that the trajectory stays behind the designed one. On the other hand, negative value gives information that the trajectory passes the designed one, which is more frequent for ADRC than PID. In particular cases, this phenomenon might be strongly undesired.

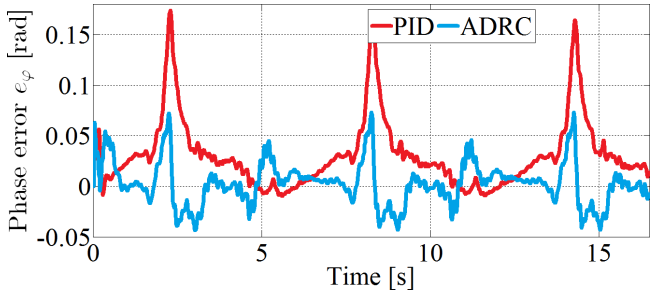

Fig. 9. Phase error e_φ for the system with basic mass (E1)

One should notice the high peaks of phase error for the PID system. They are correlated to peaks of the modulus error.

Control signal. The outputs of both the controllers are bounded within ± 12 V as mentioned in Sec. 3. The control signals for both joints are presented on Fig. 10. For the ADRC, we obtained rugged character but we can assume that the PID and ADRC do not differ much. The slight ruggedness of the ADRC control signal did not influence the manipulator motion noticeably.

Unauthenticated | 89.67.242.59
Download Date | 5/19/13 8:28 PM

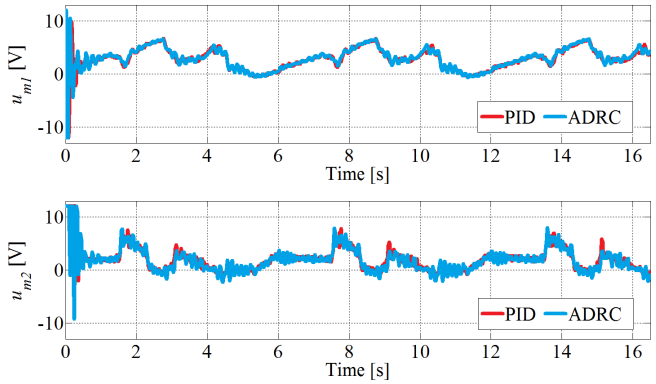

Fig. 10. Control signals of both the controllers for the system with basic mass (E1)

7.2. System with enlarged mass (E2). The graph depicting the designed trajectory together with actual paths of manipulator end effector, for both of the control methods, can be seen on Fig. 11. The difference in the performance between considered control algorithms is more noticeable this time, than in E1. The PID system has not coped well with changed system dynamics. On the other hand, ADRC executed the whole path with satisfactory result.

Again, to be able to analyze the results in a more detailed approach, we have examined three following aspects, namely: the path error, the trajectory error, and the control signal.

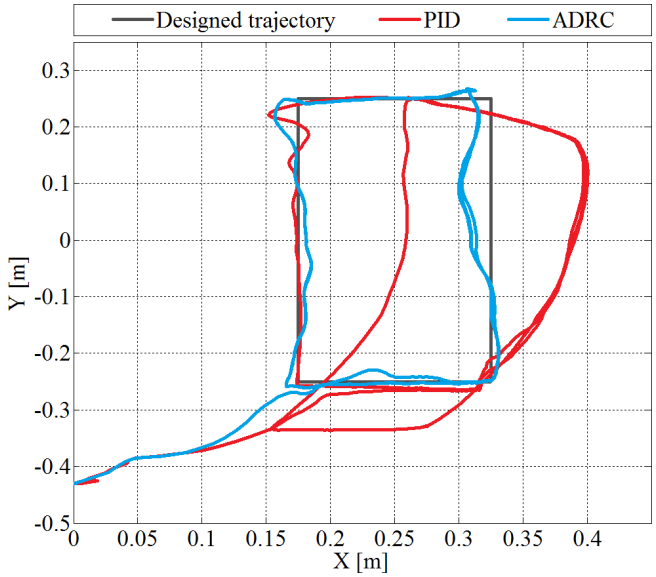

Fig. 11. Designed trajectory and actual trajectories obtained for both of the controllers in the case of system with additional mass (E2)

Path error. The CPE is presented on Fig. 12. As it can be noticed, the shape projection for both control algorithms decreased. In spite of that fact, ADRC managed to keep the shape of the path sufficiently, as the maximum absolute value of CPE increased only two times with the reference to E1. The result is acceptable, particularly when compared to CPE for PID controller, which maximum value reached more than 80 mm (the value increased eight times in relation to E1). This phenomenon can be easily concluded by comparison of values of CPE_{RMS}. For the PID it is equal to 47.12 mm and for ADRC it is 9.06 mm.

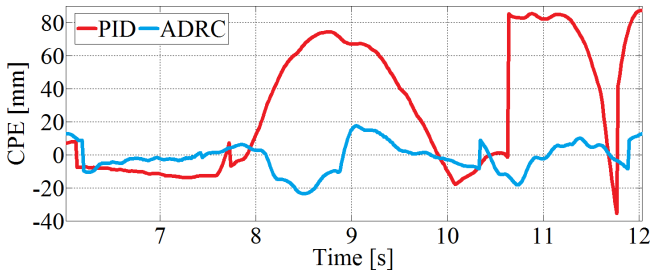

Fig. 12. Curvature projection error in the case of system with additional mass (E2)

Trajectory error. Similarly to the E1, the modulus and phase errors are calculated. The graphs can be seen on Figs. 13 and 14, respectively. The maximum value of modulus error for PID controller is greater than 1×10^{-1} m. On the contrary, ADRC error is kept within a tunnel of a similar width to the one in E1. The phase error shows that the PID control system did not perform the whole third cycle. The same graph presents that ADRC phase error is in the range of ($\varphi_{\min} = -0.2$ rad, $\varphi_{\max} = 0.11$ rad).

Even though, in the case of ADRC, shape of designed path may seem not to be projected by manipulator end effector, however the trajectory (i.e. in terms of modulus and phase) is tracked accurately.

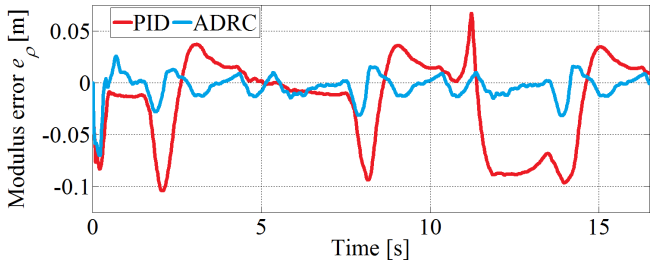

Fig. 13. Modulus error e_ρ for the system with additional mass (E2)

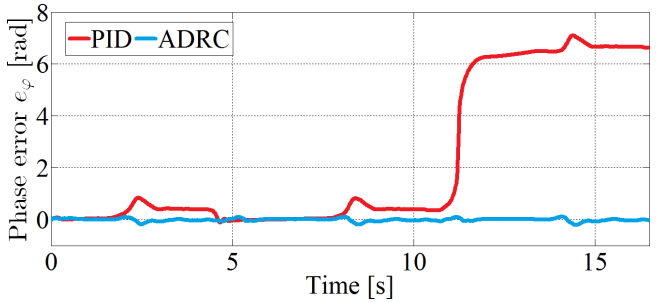

Fig. 14. Phase error e_φ for the system with additional mass (E2)

Control signal. The control signals of the PM2R for E2 are depicted on Fig. 15. The most interesting results were obtained for the second motor, since control signals for the first motor do not differ much. Therefore, only second joint control signal will be discussed.

The additional mass was directly mounted on the second joint, for that reason it is greatly influencing the dynamics

Unauthenticated | 89.67.242.59
Download Date | 5/19/13 8:28 PM

of the joint. This phenomenon, in case of PID results, was setting the control signal at the saturation level for most of the experiment time. The rugged characteristic of ADRC control signal can be noticed. Despite that, the manipulator end effector continued to follow the designed trajectory within reasonably small error tunnel. The oscillatory motion of the links was not observed here.

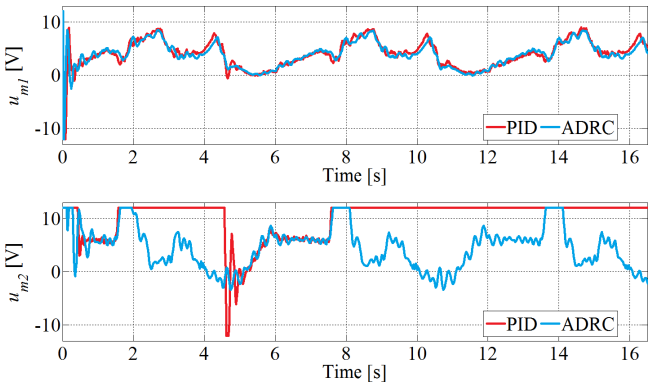

Fig. 15. Control signals of both the controllers for the system with additional mass (E2)

7.3. Discussion on ADRC. There are some aspects of the ADRC method that we found interesting during the conducted work. We think that these comments will be useful for a potential ADRC user and will provide some premises about the proper design and implementation of this control technique.

First thing that we noticed was the great importance of sampling time. The whole idea of using a disturbance observer to perform our "feedback linearization" is to estimate the uncertainties in real time. In theory, the smallest possible sampling time is thus desirable. However, we noticed two drawbacks of decreasing that time in practice. First is the presence of peaking phenomenon in which the initial estimator error is unacceptably large. This effect was analyzed minutely in [22]. Second drawback is the computation power limitation we encountered while working on the DSP board.

The ADRC can be considered as an open structure method. It means that it is up to the user to select the type feedback controller or to choose between different versions of ESO (e.g. linear or nonlinear, for details see [8]). Additionally, the knowledge about the system can be incorporated into the observer to unburden it.

Additionally, the ADRC method has the great scalability feature since it can be implemented for system of any order, whether its linear or nonlinear. It also allows one to extend the state observer and thus to estimate the consecutive derivatives of the *total disturbance*, which gives a wide range of possible applications.

In the performed experiments, the ESO was first simplified using the pole-placement method but the observer still needed empirical tuning. Other techniques can be introduced as well, including both analytical and heuristic methods (an example can be found in [25]).

8. Conclusions

This paper investigated the parametric robustness of the Active Disturbance Rejection Control method. The ADRC concept was implemented and tested on a planar manipulator with two rotational joints. It is a multi degrees-of-freedom nonlinear system with significant influence from the cross-couplings. The considered control approach was compared, in this study, to the classical PID controller. The MIMO system used in the experiments was treated as two independent plants and for each degree-of-freedom a particular controller was designed. The influence of cross-coupling effect was assumed to be unknown and it was considered as an external disturbance acting on both manipulator links. In cases of PID and ADRC, no precise modeling was used in order to tune and run the controllers. For the purpose of the experiments, control methods were first tuned and tested to give similar results in terms of tracking quality and energy efficiency (experiment E1). Then, the mass of the system was changed and experiments were repeated without any additional retuning (experiment E2).

The ADRC technique gave noticeably better results in terms of parametric robustness than PID. It was verified in both path and trajectory tracking. The Extended State Observer (ESO) effectively estimated the *total disturbance*, which in this case was the sum of modeling imprecision, unmodeled cross connections, and other system perturbations. The ADRC turned out to be a promising solution for uncertain MIMO systems giving acceptable performance with intuitive implementation and tuning.

Acknowledgements. The work was supported by grant NR13-0028/2011, funded by the Polish Ministry of Science and Higher Eduction.

REFERENCES

[1] W.S. Levine, *The Control Handbook*, CRC Press Book, London, 1999.

[2] A. Radke and Z. Gao, "A survey of state and disturbance observers for practitioners", *American Control Conf.* 1, 5183–5188 (2006).

[3] E. Schrijver and J. van Dijk, "Disturbance observers for rigid mechanical systems: equivalence, stability, and design", *J. Dynamics Systems, Measurement, and Control* 124 (4), 539–548 (2002).

[4] J.A. Profeta, W.G. Vogt, and M.H. Mickle, "Disturbance estimation and compensation in linear systems", *IEEE Trans. on Aerospace and Electronic Systems* 26 (2), 225–231 (1990).

[5] S. Kwon and W.K. Chung, "Combined synthesis of state estimator and perturbation observer", *J. Dynamics Systems, Measurement, and Control* 125 (4), 19–26 (2003).

[6] K. Youcef-Toumi and O. Ito, "A time delay controller for systems with unknown dynamics", *J. Dynamics Systems, Measurement, and Control* 112 (1), 133–142 (1990).

[7] Z. Gao, "Active disturbance rejection control: a paradigm shift in feedback control system design", *American Control Conf.* 1, 2399–2405 (2006).

[8] J. Han, "From pid to active disturbance rejection control", *IEEE Trans. on Industrial Electronics* 56 (3), 900–906 (2009).

Unauthenticated | 89.67.242.59
Download Date | 5/19/13 8:28 PM

[9] R. Madoński and P. Herman, "An experimental verification of adrc robustness on a cross-coupled aerodynamical system", *IEEE Int. Symposium on Industrial Electronics* 1, 859–863 (2011).

[10] R. Madoński, M. Przybyła, M. Kordasz, and P. Herman, "Application of active disturbance rejection control to a reel-to-reel system seen in tire industry", *Conf. on Automation Science and Engineering* 1, 274–278 (2011).

[11] G. Tian and Z. Gao, "Benchmark tests of active disturbance rejection control on an industrial motion control platform", *American Control Conf.* 1, 5552–5557 (2009).

[12] Y. Hou, Z. Gao, F. Jiang, and B.T. Boulter, "Active disturbance rejection control for web tension regulation", *Conf. on Decision and Control* 5, 4974–4979 (2001).

[13] J. Vincent, D. Morris, N. Usher, Z. Gao, S. Zhao, A. Nicoletti, and Q. Zheng, "On active disturbance rejection based control design for superconducting rf cavities", *Nuclear Instruments and Methods in Physics Research, Section* A 643 (1), 11–16 (2011).

[14] Q. Zheng, L. Dong, D.H. Lee, and Z. Gao, "Active disturbance rejection control for mems gyroscopes", *IEEE Trans. on Control Systems Technology* 17 (6), 1432–1438 (2009).

[15] M. Przybyła, R. Madoński, M. Kordasz, and P. Herman, "An experimental comparison of model-free control methods in a nonlinear manipulator", *Lecture Notes in Artificial Intelligence 7101* 1, 53–63 (2011).

[16] Z. Gao, "Scaling and bandwidth parameterization based controller tuning", *American Control Conf.* 6, 4989–4996 (2003).

[17] Q. Zheng, "On active disturbance rejection control: stability analysis and application in disturbance decoupling control", *PhD Thesis*, Cleveland State University, Cleveland, 2009.

[18] W. Zhou, S. Shao, and Z. Gao, "A stability study of the active disturbance rejection control problem by a singular perturbation approach", *Applied Mathematical Sciences* 3 (10), 491–508 (2009).

[19] Z. Gao, Y. Huang, and J. Han, "An alternative paradigm for control system design", *Conf. on Decision and Control* 5, 4578–4585 (2001).

[20] Q. Zheng, L.Q. Gao, and Z. Gao, "On estimation of plant dynamics and disturbance from input-output data in real time", *Int. Conf. on Control Applications* 1, 1167–1172 (2007).

[21] P. Kokotovic, H.K. Khalil, and J.O. Reilly, *Singular Perturbation Methods in Control Analysis and Design*, Society for Industrial and Applied Mathematics, London, 1986.

[22] H.K. Khalil, "Nonlinear output-feedback tracking using high-gain observer and variable structure control", *Automatica* 33 (10), 1845–1856 (1986).

[23] M. Michałek, "Controlling of manipulating robots", *Chair of Control and Systems Engineering*, Poznań University of Technology, Poznań, 2010 (in Polish).

[24] X. Yang and Y. Huang, "Capabilities of extended state observer for estimating uncertainties", *American Control Conf.* 1, 3700–3705 (2009).

[25] Q. Ma, D. Xu, and Y. Shi, "Research of synthesis tuning algorithm of active-disturbance-rejection controller", *World Congress on Intelligent Control and Automation* 1, 2788–2793 (2008).

Unauthenticated | 89.67.242.59
Download Date | 5/19/13 8:28 PM